ACS APPLIED MATERIALS & INTERFACES

Research Article

www.acsami.org

Solution Deposition of Thin Carbon Coatings on $LiFePO_4$

Jianxin Zhu,[†] Kevin Yoo,[‡] Ibrahim El-halees,[‡] and David Kisailus*[,†,‡]

[†]Material Science and Engineering Program, University of California−Riverside, Riverside, California 92521, United States

[‡]Department of Chemical and Environmental Engineering, University of California−Riverside, Riverside, California 92521, United States

Supporting Information

ABSTRACT: We report the synthesis of ultrathin carbon coatings on polycrystalline $LiFePO_4$ via solution deposition and subsequent annealing. The annealing temperature was systematically investigated with polymer systems on $LiFePO_4$ nanostructures. The crystal structures, sizes, and morphologies were monitored and analyzed by X-ray diffraction (XRD) and scanning electron microscopy (SEM). Micro-Raman and TEM were used to interrogate the carbon coatings after heat-treatments. Electrochemical performance of coated materials was investigated by cyclic voltammograms (CVs) and galvanostatic charge−discharge analysis. The olivine structured $LiFePO_4$ remained stable up to 600 °C but underwent a rapid reduction reaction from $LiFePO_4$ to Fe_2P above 700 °C. The good compatibility between polyethylene glycol (PEG) and the surface of $LiFePO_4$ enabled the formation of core−shell structure, which was transformed into a thin carbon coating on $LiFePO_4$ after annealing. Both PEG and sucrose carbon-based sources yielded high-quality carbon coatings after annealing, as determined by the graphitic/disordered (G/D) ratios of 1.30 and 1.20, respectively. By producing more uniform and coherent coatings on $LiFePO_4$ particles, batteries with significantly less carbon (i.e., 0.41 wt %) were fabricated and demonstrated comparable performance to traditionally synthesized carbon-coated $LiFePO_4$ with higher carbon loadings (ca. 2.64 wt %). This will enable development of batteries with higher active material loading and therefore significantly larger energy densities.

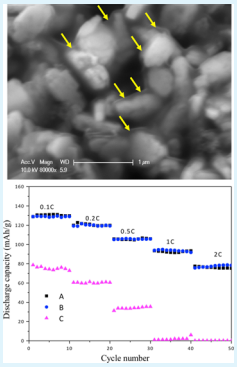

KEYWORDS: *lithium ion battery, conductive coatings, solution deposition, electrochemical performance, graphite, energy density*

1. INTRODUCTION

In 1991, Sony commercialized the first lithium-ion battery, which used carbon as the anode and $LiCoO_2$ as the cathode. Since then, a large amount of effort has been expended in the past two decades to improve the battery performance in terms of the energy density and rate capacity from both anode and cathode aspects. These improvements on anode research range from the introduction of using Si nanowires[1] to using metal oxide hollow structures,[2−5] nanoparticles,[6] nanofibers,[7] and thin films.[8] Here, we focus on a cathode, LiFePO4, which is an important component in a Li-ion batteries. Olivine-structured $LiFePO_4$ was reported by Goodenough et al.[9] in 1996 as an excellent candidate for the next-generation of large-scale lithium ion batteries for hybrid electric vehicles (HEVs) or electric vehicles (EVs) because of its low cost, nontoxic and environmentally benign nature, thermal and chemical stability, and good cyclability. One drawback of using $LiFePO_4$ (LFP) is its low rate capacity, which is due to the poor electronic conductivity and low lithium ion diffusivity. These disadvantages inhibit its broader commercial utilization. One way to overcome this inherent deficiency is to reduce the path length for Li-ion diffusion by reducing the particle size. Alternatively, the conductivity of the particles is modified by either coating the surface (e.g., with carbon or silver) or by doping the lattice (i.e., cationic/anionic doping). Among all of the different surface modifications, carbon-coated LFP has been the most intensively studied.[10−15] Previous research on carbon-coated materials has proven successful to improve battery performance. However, small amounts of carbon additive will result in the unrealistically low energy density, yielding impractical use. For example, Chen et al.,[12] determined that the addition of 2.5 wt % carbon would reduce the tap density from 1.9 to 1.05 g/cm,[3] resulting in more than 40% reduction in volumetric density. Therefore, extremely low (less than 1 wt %) carbon additives are desired. In addition to the amount of carbon, its structure can affect performance in batteries. Increasing the ratio of sp^2- (graphitic) to sp^3- (disordered) carbon will benefit the electronic conductivity.[14] Thus, it is urgent to produce high-quality graphitic carbon coatings with minimal loading. Here, we disperse cathode materials in a polymer solution, which subsequently yields thin and uniformly polymer-coated particles that are annealed to form carbon coatings. This is advantageous over conventional mechanochemical activation methods that produce heterogeneous and thick carbon coatings. We utilize a polyethylene glycol (PEG) polymer as the carbon source to coat the polycrystalline LFP reported previously.[16] Aqueous-based polyethylene glycol solutions have been widely used.[17] Their low toxicity and volatility, as well as their biodegradability, represent important environmentally benign characteristics, which are particularly attractive when

Received: September 24, 2014
Accepted: November 11, 2014
Published: November 11, 2014

 © 2014 American Chemical Society

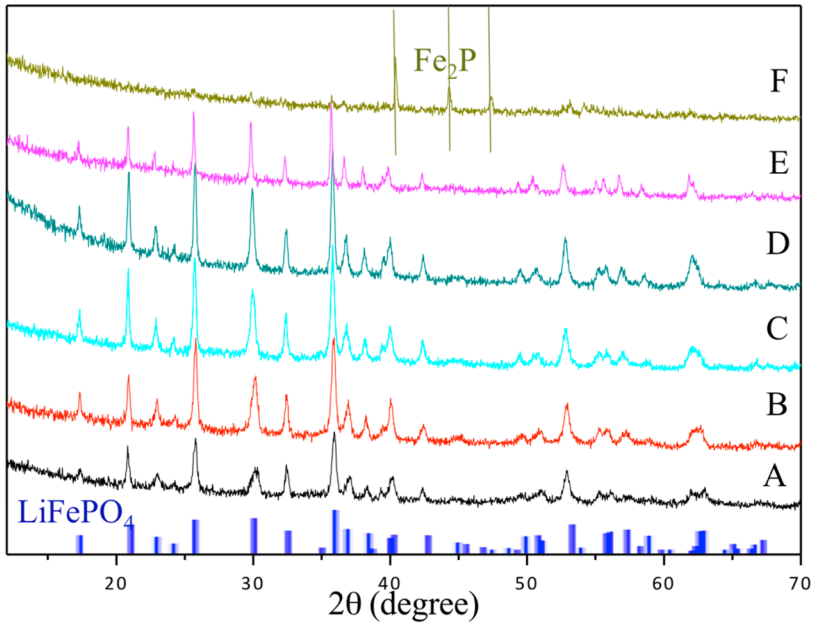

Figure 1. X-ray diffraction patterns for as-synthesized LFP annealed for 3 h in 95% N_2/5% H_2 at (A) 200, (B) 300, (C) 400, (D) 500, (E) 600, and (F) 700 °C.

combined with their relatively low cost as a bulk commodity chemical. Here, we use PEG as a surfactant in LFP suspensions to form core−shell structures, subsequently transforming the surface to a thin coating with very low (less than 0.5 wt %) carbon content after annealing. We compare the electrochemical performance of this material to a sucrose-based carbon coated LFP.

2. EXPERIMENTAL SECTION

2.1. Annealing of $LiFePO_4$ Powders. Solvothermally synthesized polycrystalline LFP powders[16] were ground with a mortar and pestle prior to annealing. The ground powder was placed in an alumina boat and heated in a sealed tube furnace in 95% N_2/5% H_2, forming gas at 20 cc/min from 200 °C − 700 °C for 3 h, and subsequently cooled to room temperature for characterization and electrochemical analysis. The forming gas aided in the reduction of residual Fe^{3+} (to yield Fe^{2+}) in the as-synthesized LFP.

2.2. Carbon Coating. To produce uniformly coated particles, we used a polymer solution-based method (Sample A). Briefly, a 10% PEG solution was prepared by dissolving a specific amount of polymer in degassed Milli-Q water until a clear solution formed. Concurrently, a 1 wt % LFP suspension was made by adding a specific quantity of LFP powder to degassed Milli-Q water and sonicated for 3 min. The LFP suspension was then added drop-by-drop to a stirred polymer solution at room temperature for 1 h to completely mix the polymer and LFP particles. The mixed suspension was then centrifuged at 8000 rpm for 5 min and dried in vacuum at 70 °C for 5 h. The dried samples were then placed in an alumina boat and annealed in a sealed tube furnace under 20 cm^3/min flowing 95% N_2/5% H_2 forming gas at 600 °C for 3 h.

To produce carbon-coated particles using a traditional solid-state method (Sample B), we weighed and mixed as-synthesized LFP powders and sucrose (10 wt %) in a glass jar containing alumina beads (weight ratio of alumina beads to LFP/sucrose powder was 20:1). This mixture was mechanically ground for 30 h using a rolling instrument. After being ground, the mixture was placed in an alumina boat and annealed in an alumina tube furnace under 20 cm^3/min flowing 95% N_2/5% H_2 forming gas at 600 °C for 3 h.

A control specimen (Sample C), which did not contain carbon, was produced by annealing polycrystalline LFP under the same conditions as Samples A and B (i.e., at 600 °C under 20 cm^3/min flowing 95% N_2/5% H_2 forming gas for 3 h).

2.3. Material Characterization. Phase identification was determined by X-ray diffraction analysis (XRD, Philips X'Pert) using Cu Kα radiation. Using the resulting XRD diffraction patterns, we calculated the crystallite diameters based on the Scherer formula.[18] We observed particle sizes and morphologies using a scanning electron microscope (SEM, FEI XL30) at 10−20 kV accelerating voltage. To investigate the behavior of LFP during annealing, we performed thermal and mass analyses using a thermal gravimetric analyzer/differential scanning calorimeter (TGA/DSC, TA Instruments Q600), annealed from 25 to 700 °C (heating rate of 10 °C/min) with a 3 h hold at 700 °C in 95% N_2/5% H_2. Raman spectroscopy measurements were carried out at room temperature under ambient conditions using a 532 nm laser as the excitation source at 1 mW power. The total carbon content of coated LFP samples was analyzed using a PerkinElmer 2400 II CHN analysis from Tucson Laboratory of ALS (Australian Laboratory Services) environmental center. A transmission electron microscope (TEM, FEI CM300), operated at 300 kV, was used to identify the carbon coating thickness.

2.4. Electrochemical Performance. As-prepared LFP powders (either samples A, B or C), conductive carbon black (Super P), and polyvinylidene fluoride (PVDF, 78:14:8 wt %) were mixed in *N*-methylpyrrolidone (NMP) to produce a slurry. This viscous slurry was subsequently coated on an aluminum foil current collector. The coated film was dried in the vacuum oven at 100 °C for 12 h. Coin cells (R2032 type) were assembled in an argon-filled glovebox, consisting of the prepared positive electrode, lithium metal foil as the negative electrode, Celgard polymer as a separator and 1.0 M $LiPF_6$ in ethylene carbonate (EC)−diethyl carbonate (DEC) (50:50 vol %) as the electrolyte solution. The loading of the active material was 1.5−2 mg/cm^2. The cyclic performance and rate capability of LFP batteries were tested using an Arbin battery test system (Arbin Instruments, Model BT2043). Cyclic voltammograms were run on a VMP3 multichannel electrochemical station.

3. RESULTS AND DISCUSSION

3.1. Annealing. *3.1.1. Thermal Behavior of $LiFePO_4$.* To obtain an optimum annealing temperature for the carbon coating process, we investigated the thermal behavior of synthesized polycrystalline LFP by TGA/DSC (Figure S1,

Supporting Information). Thermal analyses revealed that the synthesized polycrystalline LFP was stable beyond 600 °C but underwent a reduction reaction above 700 °C in 95% N_2/5% H_2.[19] Based on these results, we systematically investigated the effects of annealing at different temperatures (i.e., from 200 to 700 °C) on the resulting crystalline and particle structures. XRD (Figure 1) of LFP annealed between 200 and 600 °C confirmed the presence and stability of the orthorhombic olivine-type structure (JCPDS# 81-1173)[20] and significant crystal growth above 500 °C. Corroborating evidence of an increase in crystalline size above 400 °C is seen in the endothermic peaks at 398, 505, and 570 °C from the DSC curve in Figure S1, Supporting Information. The sample annealed at 700 °C for 3 h transformed to the Fe_2P phase (Figure 1), reflecting the reduction of LFP under N_2/H_2 at higher temperatures. Weight loss above 600 °C from TGA (Figure S1, Supporting Information) confirmed this transformation.

Morphological changes were also observed (Figure 2) for samples heat-treated at various temperatures. By 400 °C, smaller nanoparticles were not observed, and the surfaces of larger particles became smoother. By 500 °C, particle sizes decreased with increasing crystallite size, and the particles appeared more rounded. By 600 °C, the diamond-like morphology of particles was no longer evident, and some faceting was observed. By 700 °C, a clear change in particle size and morphology had occurred. XRD of this sample (Figure 1F) confirmed the Fe_2P phase, explaining this significant change. The apparent decrease in secondary particle size upon annealing from 200 to 600 °C can be explained based on the initial formation mechanism of LFP under hydro-solvothermal methods.[16] After nucleation, the charge on primary particles decreases, allowing their approach to each other, eventually yielding polycrystalline secondary particles via oriented attachment, but with some porosity. During annealing, we see an increase in crystal size (peak sharpness from Figures 1C–E) and a decrease in the number of grain boundaries per particle (eventually yielding more single crystal-like particles; Figure 2E).

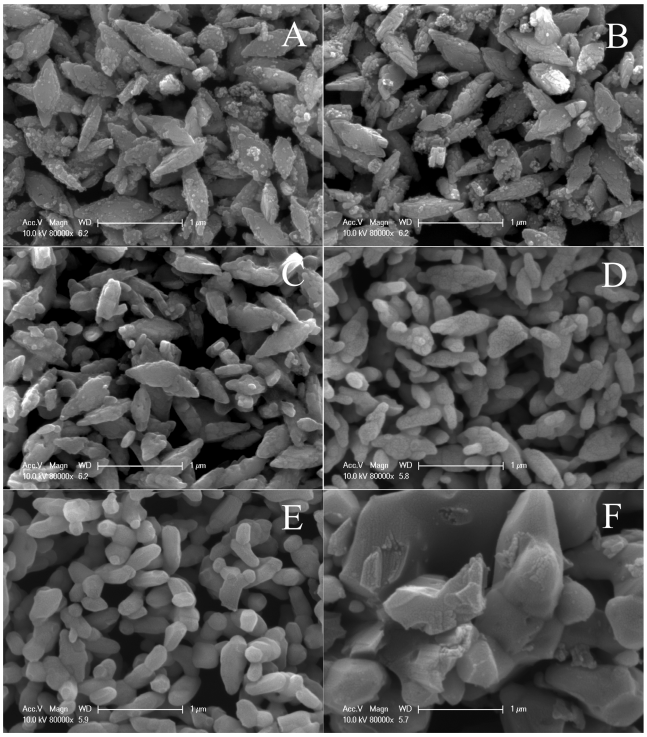

Figure 2. SEM micrographs of as-synthesized LFP annealed in 95% N_2/5% H_2 for 3 h at (A) 200, (B) 300, (C) 400, (D) 500, (E) 600, and (F) 700 °C.

3.1.2. Thermal Behavior of PEG and Sucrose. Thermal analyses of polyethylene glycol and sucrose additives, heated in 95% N_2/5% H_2 from 25 to 700 °C were investigated using TGA/DSC (Figure S2, Supporting Information). PEG starts to decompose at ~225 °C, and its decomposition is completed by 400 °C with only a small amount of carbon remaining (0.5 wt %).[21] A similar TGA/DSC trend was also observed for sucrose, initiating at 225 °C, but degrading more slowly over a broader temperature range. To analyze the resulting carbon structure, we conducted micro-Raman analyses for residues after various heat treatments for both PEG and sucrose sources.

Raman has been widely used to detect and differentiate graphitic versus disordered carbon. Graphitized carbon is known to have a better electronic conductivity compared to disordered carbon.[22−29] On the basis of observations from TGA/DSC (Figure S2, Supporting Information), we annealed PEG samples in 95% N_2/5% H_2 (20 cc/min) at four temperatures (400, 500, 600, and 700 °C) for 3 h to investigate the resulting ordering in the resulting carbon structures (Figure S3, Supporting Information). All of the Raman spectra (Figure S3, Supporting Information) consist of two intense peaks at 1355 and 1584 cm^{-1}, corresponding to the disordered (D) and graphitic (G) bands of carbon, respectively. The third broad peak at 2710 cm^{-1} is attributed to the 2D band (D peak overtone), which originates from a process where momentum conservation is satisfied by two phonons with opposite wave vectors.[30] It is clear that for all samples, the graphitic peak at 1584 cm^{-1} showed a higher intensity compared to the disordered carbon peak at 1355 cm^{-1}, indicating a good expected electronic conductivity.[26,28] Upon careful examination of these peaks, we found a trend in the ratio of G/D (Table S1Supporting Information). The G/D ratio increased from 400 to 600 °C, then decreased at 700 °C. The decreased graphitic peak intensity ratio is due to the disruption of layered carbon structure at high temperatures in the forming gas (the exothermic peak at 600 °C in Figure S2, Supporting Information).[31]

On the basis of an increasing ratio of G/D from 500 to 600 °C for sucrose (Figure S4, Supporting Information), we chose an annealing temperature of 600 °C for carbon coatings on LFP.

3.2. Carbon-Coated $LiFePO_4$ from PEG (Sample A). *3.2.1. PEG Solution-based Coatings.* The morphology of coated particles (as-synthesized polycrystalline LFP suspension mixed with the PEG solution, section 2.2), were studied via SEM. Figure 3 reveals that the surfaces of LFP were surrounded by a ~50 nm organic coating (i.e., PEG thin film) that, upon heating, yielded an evenly distributed carbon layer. The uniformity with which PEG coats the LFP particles can be explained by their interactions. The solution pH of 1 wt % LFP in water is ~10.5 (caused by the reaction of Li with water[32]). Thus, the surfaces of LFP will be negatively charged (from previous zeta potential results of LFP[16]). Aqueous PEG solutions (10 wt %) have a pH = 7.3. Based on the pK_a value of PEG (14−16), we expect the polymers to be positively charged, and thus it can electrostatically bind with the LFP

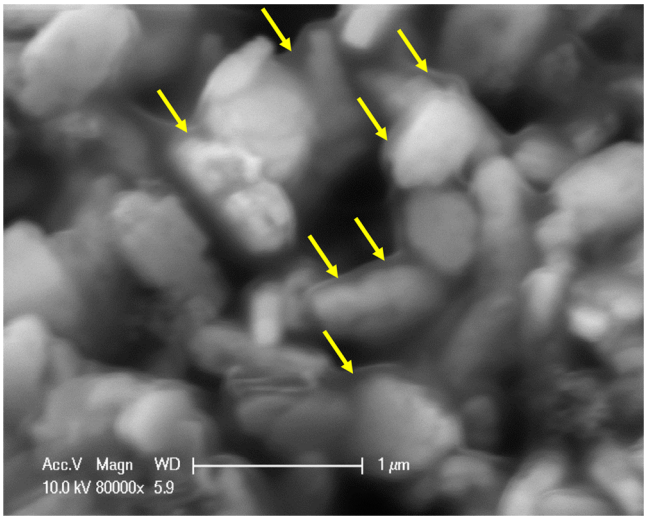

Figure 3. SEM micrograph of solution-coated PEG on as-synthesized LFP.

surface. In addition, synthesis of these particles (i.e., using a mixed hydro-solvothermal method), would likely lead to a high density of hydroxyl groups bound to the surface of the LFP. These surface hydroxyls would enable hydrogen bonding with the PEG functional groups, leading to a more conformal coating.

3.2.2. Carbon-Coated LFP from PEG. After the LFP was coated with PEG, samples were annealed at 600 °C in forming gas for 3 h. SEM micrographs (Figure 4) display a similar

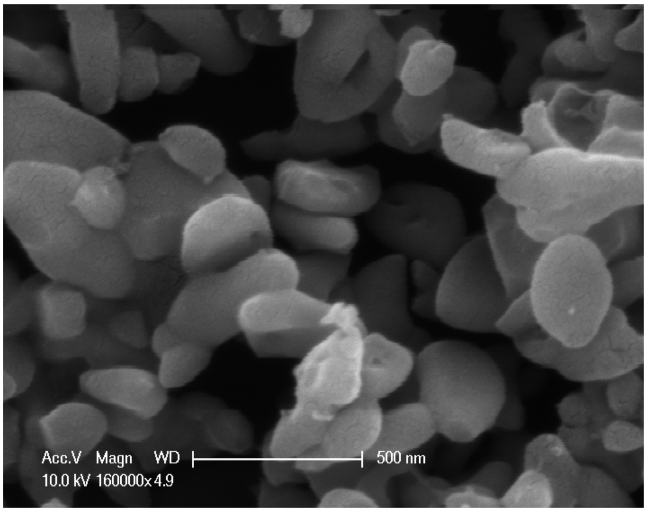

Figure 4. SEM micrograph of carbon-coated LFP (from PEG) after annealing at 600 °C for 3 h in 95% N_2/5% H_2 at 20 cc/min.

morphology as the as-synthesized LFP[16] but with a reduction in smaller nanoparticles and grain boundaries. This is likely due to sintering of smaller grains during annealing. XRD (Figure 5) confirms the material is pure LFP without any detectable impurities (e.g., such as FeP or Fe_2P). The crystallite size of the LFP, coated with polymer, was calculated to be 52 nm using the Scherer equation (Table 1).

Raman analysis (Figure 6) of the resulting carbon structure for PEG-coated LFP after annealing reveals that the G/D ratio is the same (1.30) as pure PEG heat-treated under the same conditions and is comparable or even better than previous

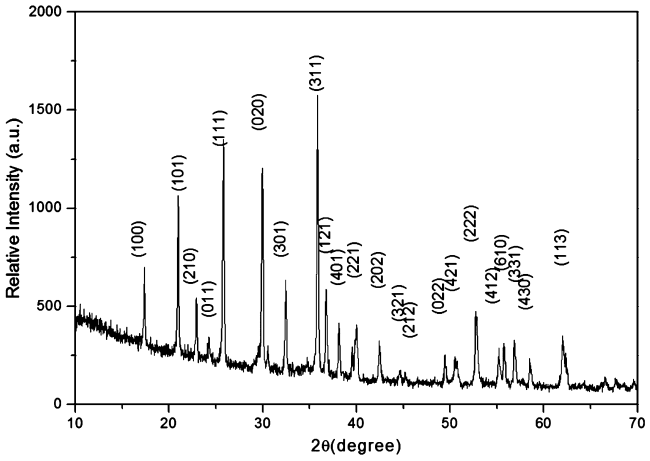

Figure 5. X-ray diffraction pattern of PEG-based LFP after annealing at 600 °C for 3 h in 95% N_2/5% H_2 at 20 cc/min.

Table 1. Crystal Size and Carbon Content for Samples A, B, and C after Heat Treatment in 95% N_2/5% H_2 at 600°C for 3 h

sample	polymer added	crystal size (nm)	particles size (nm)	carbon content after annealing (wt %)
A	PEG added	52	457 nm ±154	0.41
B	sucrose (wt. 10%) added	41	340 nm ±180	2.64
C	control (w/o polymer)	81	488 nm ±94	0

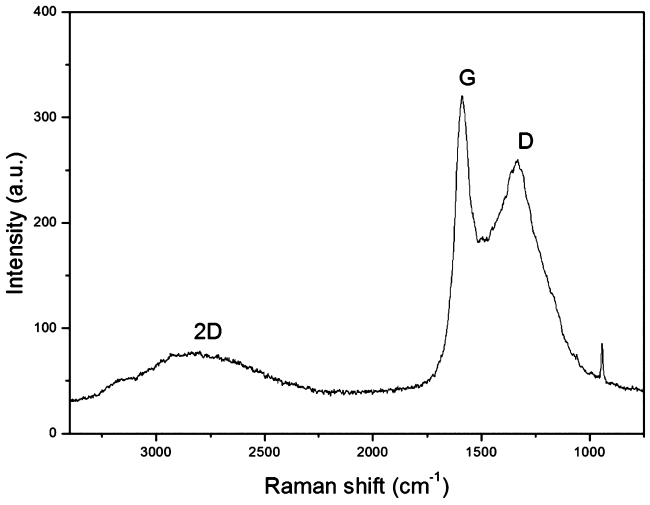

Figure 6. Raman spectrum of PEG-based LFP after annealing at 600 °C for 3 h in 95% N_2/5% H_2 at 20 cm^3/min.

reports.[14,33,34] The less intense peak at 946 cm^{-1} is ascribed to the symmetric vibration of the PO_4 groups in LFP.[33] On the basis of the high ratio of graphitic carbon to disordered carbon, we expected these coated LFP particles to display good electronic conductivity, with better high-rate discharge capacities in cells. TEM observations (Figure S5, Supporting Information) of this sample were conducted to probe the coating structure. The outer surface of the particle contains a very thin coating (~1−2 nm thick, highlighted by arrows). Raman spectroscopy, which probes a significantly larger volume of material than by TEM, showed a relatively high graphitic-to-disordered ratio, and it is therefore likely that a large fraction of

these coatings is graphitic. However, the potential orientation of the graphite within these coatings is unknown and further investigations are in progress.

3.3. Carbon-Coated $LiFePO_4$ from Sucrose (Sample B). Sucrose, a commonly used source of carbon in battery materials, was also selected to investigate its effect as a carbon coating on the polycrystalline LFP. As mentioned previously, sucrose was mechanically mixed with LFP and subsequently annealed in forming gas to 600 °C (the same as PEG-coated LFP). Figure 7 shows that particles tend to be more aggregated compared to the PEG added LFP, which is likely due to heterogeneities from a solid-state mixing process, whereas the solution method utilized a homogenized suspension of LFP particles.

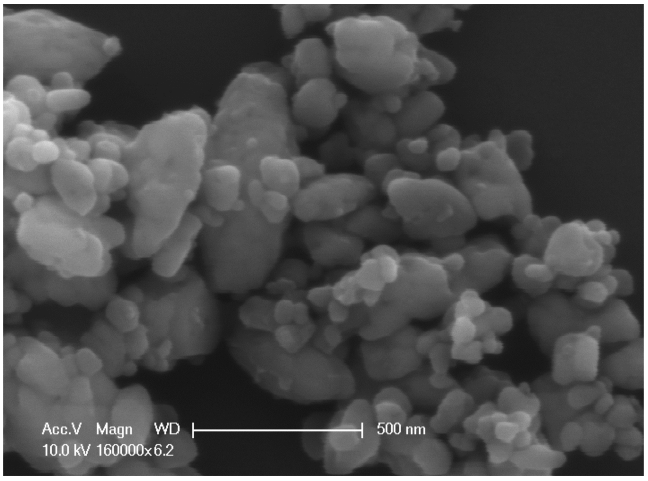

Figure 7. SEM micrograph for sucrose-added LFP mixture after annealing at 600 °C for 3 h in 95% N_2/5% H_2 at 20 cc/min.

XRD (Figure S6, Supporting Information) confirmed pure LFP without any detectable impurities. The crystal size was calculated to be 41 nm (as determined from the Scherer equation; Table 1), which is smaller compared to the PEG-added LFP. This difference in crystallite size is likely due to the extra energy provided for crystal growth by the exothermic decomposition of PEG (Figure S2, Supporting Information). Specifically, there is an exothermic peak at 425 °C in PEG but no exothermic peak observed in the decomposition of sucrose.

Raman spectroscopy (Figure S7, Supporting Information) uncovers the resulting carbon structure for the sucrose-based, carbon-coated LFP after annealing in forming gas to 600 °C. The spectrum is very similar to the PEG-based carbon-coated LFP, with a slightly lower G/D ratio of 1.20.

To determine carbon content in annealed samples, we performed CHN analyses on samples A and B (Table 1). The carbon content in sample A (PEG-based carbon coated LFP) is only 0.41 wt % compared to 2.64 wt % carbon in sample B (sucrose added LFP). Thus, the tap density should be greater for sample A, which would increase the energy density of constructed batteries. In addition, the PEG-based carbon-coated LFP showed a high concentration of graphitic carbon and had small crystallite sizes and an evenly distributed particle size, which should display excellent electrochemical performance.

A carbon-free LFP (sample C), heat-treated at 600 °C for 3 h in 95% N_2/5% H_2 at 20 cc/min, was used as a control. XRD (Figure 1E) confirmed the pure LFP phase and SEM (Figure

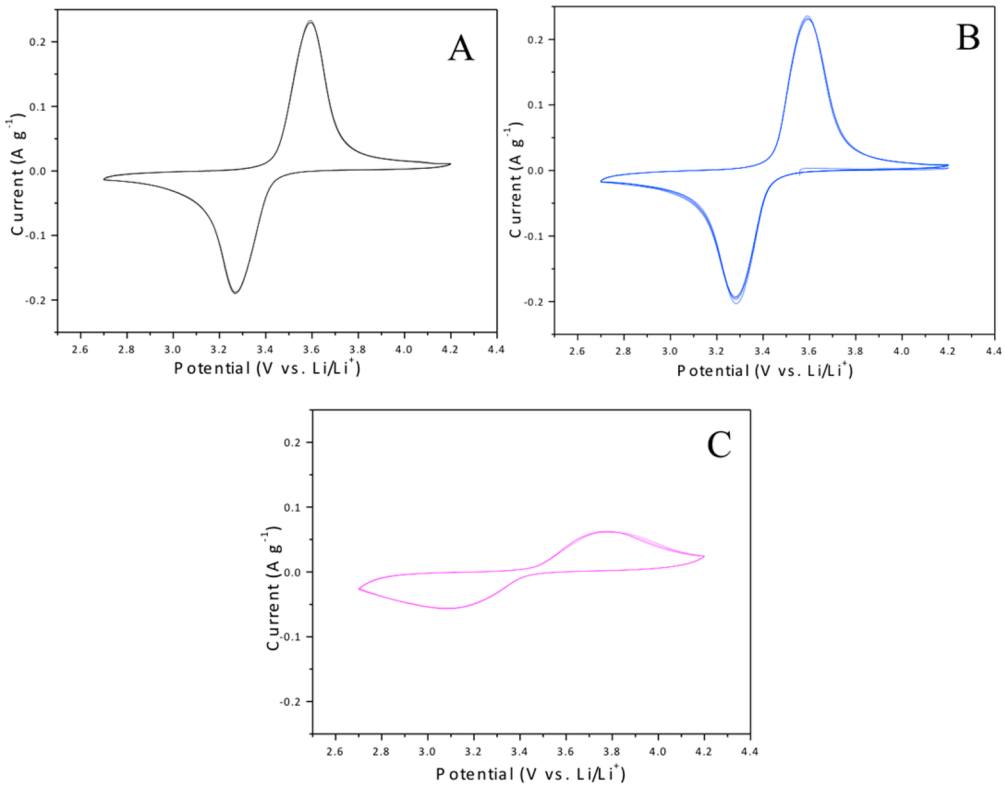

Figure 8. CV profiles of LFP in the voltage range of 2.7−4.2 V at a scan rate of 0.1 mV/s for (A) PEG-based carbon-coated LFP, (B) sucrose-based carbon-coated LFP, and (C) uncoated LFP control.

dx.doi.org/10.1021/am506498p | ACS Appl. Mater. Interfaces 2014, 6, 21550−21557

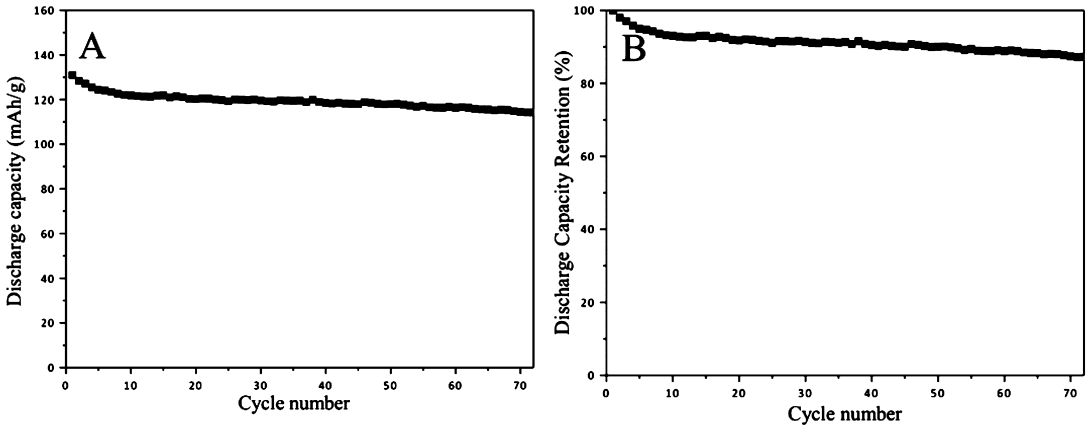

Figure 9. Discharge capacity vs cycle number for PEG-based carbon-coated LFP. (A) Cycling performance at 0.1 C between 2.7 and 4.2 V (vs Li^+/Li) for 70 cycles, (B) discharge capacity retention.

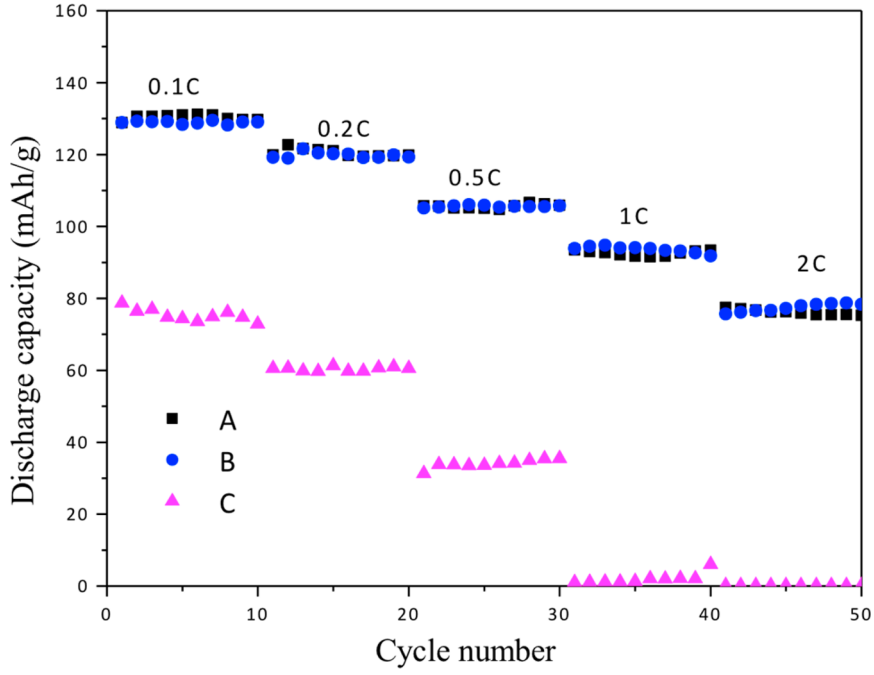

Figure 10. Carbon-coated and carbon-free LFP cycling performance at various current rates between 2.7 and 4.2 V (vs Li^+/Li). (A) PEG-based carbon-coated LFP, (B) sucrose-based carbon-coated LFP, and (C) uncoated LFP control.

2E) revealed a decrease in particle size along with an increased crystal size (Table 1).

3.4. Electrochemical Performance of $LiFePO_4$. *3.4.1. Cyclic Voltammetry.* Cyclic voltammetry (CV) (Figure 8), performed on all samples at a scan rate of 0.1 mV/s at room temperature for three cycles, displays an oxidation peak and a reduction peak, corresponding to the charge/discharge reactions of the Fe^{2+}/Fe^{3+} redox couple. Each of the second and third scans display similar profiles as the first, suggesting the good reversibility of these cathodes. The PEG-based carbon-coated LFP (sample A) displayed a voltage hysteresis of 0.32 V with a peak current of 0.23 A/g, while the carbon-free LFP (control sample C) had a voltage difference of 0.60 V and a peak current of 0.11 A/g. It is known that smaller voltage differences between the charge and discharge, as well as higher peak currents, indicate better electrode reaction kinetics and thus better rate performance.[35,36] The results demonstrate that carbon-coated LFP have enhanced kinetics compared to carbon-free LFP during the lithiation and delithiation due to the increased electronic conductivity through carbon coating. A comparison of carbon-coated samples A and B reveals a similar voltage hysteresis (0.32 V for sample A and 0.31 V for sample B) and the same peak current (0.23 A/g for both A and B), indicating similar kinetic behavior, even though sample A has a much lower carbon content (0.41%) compared to sample B (2.64%). Thus, our solution-processed carbon coating yields impressive performance but will have greater enhanced tap density and thus a higher volumetric energy density.

3.4.2. Charge/Discharge Capacity. Figure 9 shows the galvanostatic discharge capacity as a function of cycle number for carbon-coated LFP (sample A) at a current density of 16 mA/g. The cells can deliver 130 mAh/g capacity after 70 cycles with ~92% capacity retention (Figure 9B), indicating excellent cycle stability. It was reported that very small (<2%) amounts of carbon can effectively increase the capacity retention.[34] Here,

with less than 0.5% carbon in our LFP, the capacity retention was increased dramatically.

The specific discharge capacities at different current rates (from 16 mA/g to 320 mA/g) for samples A, B, and C are shown in Figure 10. Uncoated LFP (sample C) delivers 115 mAh/g at 0.1 C, which is better than the other reported data for carbon-free LFP (60 mA h/g at 0.1 C).[37] After coating with 0.41 wt % carbon, the capacity significantly increased (black ■). The remarkable advantage of this carbon-coated material is its high rate capability (80 mA h/g at 2C) with extremely low carbon content. Its performance is comparable with the 2.64 wt % coated LFP (blue ●). Thus, with low quantities of carbon additive, the tap density of LFP increased from 1.1 to 1.8 g/cm^3 with a 40% increase in volumetric density.

4. CONCLUSIONS

We have successfully applied a thin carbon coating on LFP via a polyethylene glycol solution method. The core−shell structure was formed due to electrostatic absorption of the polymer onto LFP particles and was subsequently transformed into a thin carbon coating upon heat treatment in N_2/H_2. Less than 0.5 wt % of a multilayer graphitic coating greatly increased the electronic conductivity and, therefore, the enhanced electrochemical performance. It is very promising for many applications because the carbon additive does not affect the theoretical volumetric energy and has an increased tap density compared to other high-carbon-content (∼3 wt %) cathodes.

■ ASSOCIATED CONTENT

Supporting Information

Data describing the thermal behavior of the $LiFePO_4$ and carbon-based coatings, as well as their structural features, including thermal behavior of as-synthesized $LiFePO_4$ (S1), PEG (S2A) and sucrose (S2B) from 25 to 700 °C under 20 cm^3/min 95% N_2/5% H_2; structural carbon data (Table S1) from PEG (S3) and sucrose (S4) that are annealed at different temperatures; PEG-based carbon-coatings on LFP are observed (S5) and structural data from annealed sucrose-coated LFP (S6, S7). This material is available free of charge via the Internet at http://pubs.acs.org.

■ AUTHOR INFORMATION

Corresponding Author

*E-mail: david@engr.ucr.edu. Phone: +1-951-827-4310. Fax: +1-951-827-5696.

Notes

The authors declare no competing financial interest.

■ ACKNOWLEDGMENTS

We would like to acknowledge funding from Winston Chung Global Energy. We also thank Professor Juchen Guo for use of his electrochemical facilities.

■ REFERENCES

(1) Chan, C. K.; Peng, H.; Liu, G.; McIlwrath, K.; Zhang, X. F.; Huggins, R. A.; Cui, Y. High-Performance Lithium Battery Anodes Using Silicon Nanowires. *Nat. Nanotechnol.* **2008**, *3*, 31−35.

(2) Lou, X. W.; Wang, Y.; Yuan, C.; Lee, J. Y.; Archer, L. A. Template-Free Synthesis of SnO_2 Hollow Nanostructures with High Lithium Storage Capacity. *Adv. Mater.* **2006**, *18*, 2325−2329.

(3) Lai, X.; Halpert, J. E.; Wang, D. Recent Advances in Micro-/Nano-Structured Hollow Spheres for Energy Applications: From Simple to Complex Systems. *Energy Environ. Sci.* **2012**, *5*, 5604−5618.

(4) Wang, J.; Yang, N.; Tang, H.; Dong, Z.; Jin, Q.; Yang, M.; Kisailus, D.; Zhao, H.; Tang, Z.; Wang, D. Accurate Control of Multishelled Co_3O_4 Hollow Microspheres as High-Performance Anode Materials in Lithium-Ion Batteries. *Angew. Chem., Int. Ed.* **2013**, *52*, 6417−6420.

(5) Xu, S.; Hessel, C. M.; Ren, H.; Yu, R.; Jin, Q.; Yang, M.; Zhao, H.; Wang, D. α-Fe_2O_3 Multi-Shelled Hollow Microspheres for Lithium Ion Battery Anodes with Superior Capacity And Charge Retention. *Energy Environ. Sci.* **2014**, *7*, 632−637.

(6) Wu, Z. S.; Ren, W.; Wen, L.; Gao, L.; Zhao, J.; Chen, Z.; Zhou, G.; Li, F.; Cheng, H.-M. Graphene Anchored with Co_3O_4 Nanoparticles as Anode of Lithium Ion Batteries with Enhanced Reversible Capacity and Cyclic Performance. *ACS Nano* **2010**, *4*, 3187−3194.

(7) Zou, M.; Li, J.; Wen, W.; Chen, L.; Guan, L.; Lai, H.; Huang, Z. Silver-Incorporated Composites of Fe_2O_3 Carbon Nanofibers as Anodes for High-Performance Lithium Batteries. *J. Power Sources* **2014**, *270*, 468−474.

(8) Polat, D. B.; Keles, O.; Amine, K. Well-Aligned, Ordered, Nanocolumnar, Cu-Si Thin Film as Anode Material for Lithium-Ion Batteries. *J. Power Sources* **2014**, *270*, 238−247.

(9) Padhi, A. K.; Nanjundaswamy, K. S.; Goodenough, J. B. Phospho-Olivines as Positive-Electrode Materials for Rechargeable Lithium Batteries. *J. Electrochem. Soc.* **1997**, *144*, 1188−1194.

(10) Wu, X. L.; Jiang, L. Y.; Cao, F. F.; Guo, Y. G.; Wan, L. J. $LiFePO_4$ Nanoparticles Embedded in a Nanoporous Carbon Matrix: Superior Cathode Material for Electrochemical Energy-Storage Devices. *Adv. Mater.* **2009**, *21*, 2710−2714.

(11) Dominko, R.; Bele, M.; Gaberscek, M.; Remskar, M.; Hanzel, D.; Pejovnik, S.; Jamnik, J. Impact of the Carbon Coating Thickness on the Electrochemical Performance of $LiFePO_4$/C Composites. *J. Electrochem. Soc.* **2005**, *152*, A607−A610.

(12) Chen, Z. H.; Dahn, J. R. Reducing Carbon in $LiFePO_4$/C Composite Electrodes to Maximize Specific Energy, Volumetric Energy, and Tap Density. *J. Electrochem. Soc.* **2002**, *149*, A1184−A1189.

(13) Yuan, L. X.; Wang, Z. H.; Zhang, W. X.; Hu, X. L.; Chen, J. T.; Huang, Y. H.; Goodenough, J. B. Development and Challenges of $LiFePO_4$ Cathode Material for Lithium-Ion Batteries. *Energy Environ. Sci.* **2011**, *4*, 269−284.

(14) Doeff, M. M.; Hu, Y. Q.; McLarnon, F.; Kostecki, R. Effect of Surface Carbon Structure on the Electrochemical Performance of $LiFePO_4$. *Electrochem. Solid State Lett.* **2003**, *6*, A207−A209.

(15) Belharouak, I.; Johnson, C.; Amine, K. Synthesis and Electrochemical Analysis of Vapor-Deposited Carbon-Coated $LiFePO_4$. *Electrochem. Commun.* **2005**, *7*, 983−988.

(16) Zhu, J.; Fiore, J.; Li, D.; Kinsinger, N. M.; Wang, Q.; DiMasi, E.; Guo, J.; Kisailus, D. Solvothermal Synthesis, Development, and Performance of $LiFePO_4$ Nanostructures. *Cryst. Growth Des.* **2013**, *13*, 4659−4666.

(17) Chen, J.; Spear, S. K.; Huddleston, J. G.; Rogers, R. D. Polyethylene Glycol and Solutions of Polyethylene Glycol as Green Reaction Media. *Green Chem.* **2005**, *7*, 64−82.

(18) Alexander, L.; Klug, H. P. Determination of Crystallite Size with the X-Ray Spectrometer. *J. Appl. Phys.* **1950**, *21*, 137−142.

(19) Rho, Y.-H.; Nazar, L. F.; Perry, L.; Ryan, D. Surface Chemistry of $LiFePO_4$ Studied by Mossbauer and X-ray Photoelectron Spectroscopy and Its Effect on Electrochemical Properties. *J. Electrochem. Soc.* **2007**, *154*, A283−A289.

(20) Gangulibabu; Kalaiselvi, N.; Bhuvaneswari, D.; Doh, C. H. On the Synergistic Effect of Carbonate Anion Directed Shape Controlled Morphology and Super P Carbon in Preparing $LiFePO_4$/C Cathode with Improved Lithium Intercalation Behavior. *Int. J. Electrochem. Sci.* **2010**, *5*, 1597−1604.

(21) Fan, M.; Liang, Y.; Zhou, F.; Liu, W. Dramatically Improved Friction Reduction and Wear Resistance by in Situ Formed Ionic Liquids. *RSC Adv.* **2012**, *2*, 6824−6830.

(22) Ferrari, A. C. Raman Spectroscopy of Graphene and Graphite: Disorder, Electron−Phonon Coupling, Doping, and Nonadiabatic Effects. *Solid State Commun.* **2007**, *143*, 47−57.

(23) Goli, P.; Legedza, S.; Dhar, A.; Salgado, R.; Renteria, J.; Balandin, A. A. Graphene-Enhanced Hybrid Phase Change Materials for Thermal Management of Li-Ion Batteries. *J. Power Sources* **2014**, *248*, 37−43.
(24) Shahil, K. M. F.; Balandin, A. A. Thermal Properties of Graphene and Multilayer Graphene: Applications in Thermal Interface Materials. *Solid State Commun.* **2012**, *152*, 1331−1340.
(25) Balandin, A. A.; Ghosh, S.; Bao, W.; Calizo, I.; Teweldebrhan, D.; Miao, F.; Lau, C. N. Superior Thermal Conductivity of Single-Layer Graphene. *Nano Lett.* **2008**, *8*, 902−907.
(26) Calizo, I.; Balandin, A. A.; Bao, W.; Miao, F.; Lau, C. N. Temperature Dependence of the Raman Spectra of Graphene and Graphene Multilayers. *Nano Lett.* **2007**, *7*, 2645−2649.
(27) Guo, S.; Ghazinejad, M.; Qin, X.; Sun, H.; Wang, W.; Zaera, F.; Ozkan, M.; Ozkan, C. S. Tuning Electron Transport in Graphene-based Field-Effect Devices using Block Co-Polymers. *Small* **2012**, *8*, 1073−1080.
(28) Guo, S.; Wang, W.; Ozkan, C. S.; Ozkan, M. Assembled Graphene Oxide and Single-Walled Carbon Nanotube Ink for Stable Supercapacitors. *J. Mater. Res.* **2013**, *28*, 918−926.
(29) Wang, W.; Guo, S.; Bozhilov, K. N.; Yan, D.; Ozkan, M.; Ozkan, C. S. Intertwined Nanocarbon and Manganese Oxide Hybrid Foam for High-Energy Supercapacitors. *Small* **2013**, *9*, 3714−3721.
(30) Ferrari, A. C.; Basko, D. M. Raman Spectroscopy as a Versatile Tool for Studying the Properties of Graphene. *Nat. Nanotechnol.* **2013**, *8*, 235−246.
(31) Wood, B. J.; Wise, H. Reaction Kinetics of Gaseous Hydrogen Atoms with Graphite. *J. Phys. Chem.* **1969**, *73*, 1348−1351.
(32) Zaghib, K.; Dontigny, M.; Charest, P.; Labrecque, J. F.; Guerfi, A.; Kopec, M.; Mauger, A.; Gendron, F.; Julien, C. M. Aging of $LiFePO_4$ upon Exposure to H_2O. *J. Power Sources* **2008**, *185*, 698−710.
(33) Lin, Y.; Gao, M. X.; Zhu, D.; Liu, Y. F.; Pan, H. G. Effects of Carbon Coating and Iron Phosphides on the Electrochemical Properties of $LiFePO_4$/C. *J. Power Sources* **2008**, *184*, 444−448.
(34) Hong, S.-A.; Kim, S. J.; Kim, J.; Lee, B. G.; Chung, K. Y.; Lee, Y.-W. Carbon Coating on Lithium Iron Phosphate ($LiFePO_4$): Comparison between Continuous Supercritical Hydrothermal Method and Solid-State Method. *Chem. Eng. J.* **2012**, *198*, 318−326.
(35) Lan, Y.; Wang, X.; Zhang, J.; Zhang, J.; Wu, Z.; Zhang, Z. Preparation and Characterization of Carbon-Coated $LiFePO_4$ Cathode Materials for Lithium-Ion Batteries with Resorcinol−Formaldehyde Polymer as Carbon Precursor. *Powder Technol.* **2011**, *212*, 327−331.
(36) Xia, Y.; Zhang, W.; Huang, H.; Gan, Y.; Tian, J.; Tao, X. Self-Assembled Mesoporous $LiFePO_4$ with Hierarchical Spindle-Like Architectures for High-Performance Lithium-Ion Batteries. *J. Power Sources* **2011**, *196*, 5651−5658.
(37) Yang, S.; Zhou, X.; Zhang, J.; Liu, Z. Morphology-Controlled Solvothermal Synthesis of $LiFePO_4$ as a Cathode Material for Lithium-Ion Batteries. *J. Mater. Chem.* **2010**, *20*, 8086−8091.